



A relationship to estimate the excess entropy of mixing: Application in silicate solid solutions and binary alloys

Artur Benisek*, Edgar Dachs

Materialforschung und Physik, Universität Salzburg, Hellbrunnerstr. 34, A-5020 Salzburg, Austria

ARTICLE INFO

Article history:

Received 2 January 2012
Received in revised form 29 February 2012
Accepted 2 March 2012
Available online 7 March 2012

Keywords:

Alloys
Oxide materials
Entropy
Heat capacity
Calorimetry
Computer simulations
Anharmonic vibrations

ABSTRACT

The paper presents new calorimetric data on the excess heat capacity and vibrational entropy of mixing of Pt–Rh and Ag–Pd alloys. The results of the latter alloy are compared to those obtained by calculations using the density functional theory. The extent of the excess vibrational entropy of mixing of these binaries and of some already investigated binary mixtures is related to the differences of the end-member volumes and the end-member bulk moduli. These quantities are used to roughly represent the changes of the bond length and stiffness in the substituted and substituent polyhedra due to compositional changes, which are assumed to be the important factors for the non-ideal vibrational behaviour in solid solutions.

© 2012 Elsevier B.V. All rights reserved.

1. Introduction

The standard entropy ($S^{298.15}$) of a perfect crystal can be derived from heat capacity (C_p) measurements ranging from 0 to 298.15 K because the entropy of a perfect crystal approaches zero when the temperature approaches zero K, i.e., the configurational part of the entropy (structural disorder) is zero. The temperature dependence of the entropy is given by the integral of $C_p/T dT$ and contains mainly the vibrational part of the entropy. Beside the vibrational entropy, the integral $C_p/T dT$ may also contain magnetic, electronic and other contributions (e.g., contributions from structural phase transitions). In solid solutions, the configurational entropy is unequal to zero and the heat capacity versus composition behaviour generally deviates from a linear relationship, especially at low temperatures of ~ 50 K. This deviation gives rise to excess heat capacities of mixing and in consequence to excess vibrational entropies of mixing. These excess quantities are significant in several binary alloys [1], but also in silicate solid solutions like alkali feldspars ($\text{NaAlSi}_3\text{O}_8$ – KAlSi_3O_8), garnets ($\text{Mg}_3\text{Al}_2\text{Si}_3\text{O}_{12}$ – $\text{Ca}_3\text{Al}_2\text{Si}_3\text{O}_{12}$), and in plagioclases ($\text{NaAlSi}_3\text{O}_8$ – $\text{CaAl}_2\text{Si}_2\text{O}_8$) [2–4].

The physical nature of the excess vibrational entropy is still poorly understood. The excess entropy was correlated with the excess enthalpy of mixing in liquid binary alloys [e.g., 1, 5]. Such

a relationship was also proposed by computer simulation studies performed on alkali halide, metallic and oxide systems [6,7]. Some light was shed on the physical nature of the excess vibrational entropy by Van de Walle and Ceder [8], who gave an overview of the suggested microscopic mechanisms. Substituting an atom by another atom of different size leads to strain fields. The smaller atoms get under tension, the larger one under compression. Beside this size mismatch effect, the bond stiffness was proposed to be an important factor [9,10]. To explain these relationships, Benisek and Dachs [10] distinguished three cases for a solid solution AC–BC:

- The B–C bonds are longer and elastically stiffer than the A–C bonds. Due to the elastically stiffer nature of the B–C bonds, their inter-atomic distances will not change as much as that of the A–C bonds with varying composition. Considering the changes from the end-member structures, the increase in A–C bond length is thus more pronounced than the decrease in B–C bond length. This behaviour is illustrated in Fig. 1. Atom A will find itself in a highly enlarged structure. Hence, the A–C bonds are softened in the solid solution and consequently, the mean frequencies of the vibrations are lowered. Vibrations with lower frequencies are excited at lower temperatures, and this behaviour generates positive excess heat capacities and vibrational entropies of mixing.
- In cases where the stiffness of the A–C and B–C bonds is similar but B–C bonds are again longer than A–C ones, the magnitude of A–C bond length increase is more pronounced than the decrease in B–C bond lengths (considering bond length changes

* Corresponding author.

E-mail address: artur.benisek@sbg.ac.at (A. Benisek).

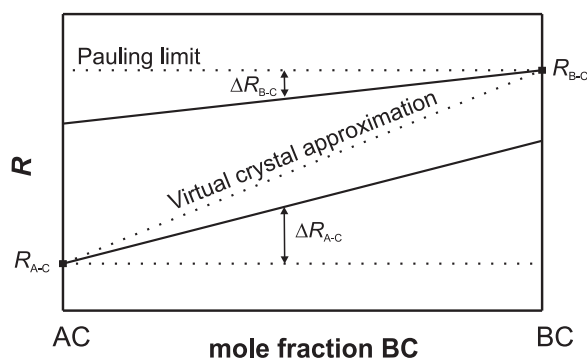


Fig. 1. Mean bond length (R) in a solid solution consisting of components AC and BC. Heavy lines show the changes of R with compositional changes. It represents cases, where the decrease of the larger polyhedron (ΔR_{B-C}) is less pronounced than the increase of the smaller one (ΔR_{A-C}). Broken lines represent the two limiting cases, Pauling limit and virtual crystal approximation.

from the end-member structures). This follows from the typical asymmetric dependence of the potential energy on the interatomic distance energetically favouring elongated bond lengths, when compared to compressed ones. Consequently, the softening of A–C bonds is again more pronounced than the stiffening of B–C bonds and positive excess heat capacities and vibrational entropies of mixing are produced.

- B–C bonds are longer but elastically softer than A–C bonds. The elastically stiffer A–C bonds force the B–C bonds to shorten to a higher extent compared to the other cases. The magnitude of bond softening may be similar to that of bond stiffening or even smaller. The effect on the entropy tends to be compensated or it results in even negative excess vibrational entropies.

Based on the cases discussed above, Benisek and Dachs [10] described the maximum values of the excess vibrational entropy ($\Delta_{\max} S^{\text{exc}}$) by relating them to the difference in the end-member volumes (ΔV_i) and to the difference in the end-member bulk moduli (ΔK_i). ΔK_i was chosen to be negative, if the end-member with the larger volume had a lower bulk modulus and vice versa. Positive, zero or negative ΔK_i values thus represented the different cases mentioned above. Although ΔV_i and ΔK_i may not reflect the actual differences in length and stiffness of A–C and B–C bonds, they were sufficient to describe $\Delta_{\max} S^{\text{exc}}$ of some silicate solid solutions.

The objective of this paper is to investigate, if this simple relationship can also be applied to binary alloys. For this purpose, two of such alloys (Ag–Pd and Pt–Rh) were investigated by relaxation and differential scanning calorimetry. To enlarge the data set, the excess entropy of mixing of binary alloys from Kubaschewski and Alcock [1] were used, where excess enthalpy, entropy and Gibbs free energy values are compiled for many binary alloys. Their entropy data were generally determined by the evaluation of calorimetric solution experiments (ΔH) and phase equilibrium experiments (ΔG).

2. Experimental methods

2.1. Relaxation calorimetry

Low temperature heat capacities were measured using a commercially available relaxation calorimeter (heat capacity option of the PPMS by Quantum Design®) from 5 to 300 K (for details of the technique, see e.g., [11] and references therein).

2.2. Differential scanning calorimetry (DSC)

High temperature heat capacities were measured using a Perkin Elmer Diamond DSC® from 280 to 800 K. The evaluation of the DSC raw data was performed as described in [12].

2.3. Binary alloys

An Ag_{69.7}Pd_{30.3} sheet (~30 mg) and a Pt_{55.2}Rh_{44.8} wire (~60 mg) were used for the calorimetric measurements. The Ag–Pd alloy was manufactured by Ögussa®, and the Pt–Rh alloy was obtained from Conatex®.

2.4. Calculations using the density functional theory (DFT)

The quantum-mechanical calculations presented here were based on the DFT plane wave pseudopotential approach using the CASTEP software [13] included in the Materials Studio software from Accelrys®. The calculations were performed using the local density approximation (LDA) [14]. Alternatively, the gradient-corrected functional (GGA-PBE) from Perdew et al. [15] was used. An ultrasoft and alternatively a norm-conserving pseudopotential were used to calculate the wavefunctions of the ion core. Lattice dynamics calculations were based on the finite displacement approach, implemented in CASTEP, which calculates the forces on perturbed configurations in a supercell with positive and negative displacements. This enables the analysis of the asymmetry of the potential well and thus the study of anharmonic effects [16]. This can be done by increasing the atomic displacement from the default value of 0.0053 Å, which corresponds to the harmonic approximation, to higher values (personnel communication with S.J. Clark, University of Durham). The heat capacities of the end-members were calculated applying the same calculation parameters and structures (i.e., super cell with P1 symmetry) as used for the solid solutions. For each substance (Ag, Pd, Ag₇₅Pd₂₅), the calculations were performed several times increasing the precision of the calculation until the excess heat capacity values converged.

3. Results and discussion

3.1. Calorimetric results on Pt–Rh and Ag–Pd alloys

The raw C_p data of Pt_{55.2}Rh_{44.8} and Ag_{69.7}Pd_{30.3} have been deposited as electronic supplementary material linked to this article. The excess heat capacity of mixing is defined as

$$\Delta C_p^{\text{exc}} = C_p^{\text{AB}} - (C_p^{\text{A}} \cdot X_A + C_p^{\text{B}} \cdot X_B) \quad (1)$$

using mole fractions (X) of components A and B. The heat capacities for the low temperature region of the end-members were taken from the National Bureau of Standards [17,18] and those for the high temperature region were taken from Barin and Knacke [19]. These data allowed the calculation of ΔC_p^{exc} from the measured heat capacity of Pt_{55.2}Rh_{44.8} and Ag_{69.7}Pd_{30.3}. The Pt_{55.2}Rh_{44.8} alloy is characterised by small negative excess heat capacities ($<0.2 \text{ J mol}^{-1} \text{ K}^{-1}$) at low temperatures ($<60 \text{ K}$) and by positive excess heat capacities (not exceeding $0.5 \text{ J mol}^{-1} \text{ K}^{-1}$) at temperatures between 60 and 800 K. The resulting excess vibrational entropy is positive and amounts to $\Delta S^{\text{exc}} = 0.5 \text{ J mol}^{-1} \text{ K}^{-1}$ at 800 K. The entropy composition behaviour along this binary was assumed to be symmetric so that a maximum excess vibrational entropy, $\Delta_{\max} S^{\text{exc}} = 0.5 \text{ J mol}^{-1} \text{ K}^{-1}$ is proposed for this binary.

The Ag_{69.7}Pd_{30.3} alloy has negative excess heat capacities below 450 K, characterised by two negative peaks at ~50 and ~270 K, shown in Fig. 2. The calculated excess vibrational entropy at 450 K is $\Delta S^{\text{exc}} = -1.4 \text{ J mol}^{-1} \text{ K}^{-1}$. Because the Ag–Pd alloy shows symmetric excess entropy behaviour [1], our calorimetrically determined value was used to calculate the maximum excess entropy for Ag–Pd alloys. Our calculations using the Margules mixing model yield $\Delta_{\max} S^{\text{exc}} = -1.7 \text{ J mol}^{-1} \text{ K}^{-1}$. This value is slightly less negative compared to the value given by Kubaschewski and Alcock [1] ($\Delta_{\max} S^{\text{exc}} = -1.84 \text{ J mol}^{-1} \text{ K}^{-1}$). Their data evaluation used the configurational entropy (S^{cfg}) of a fully disordered distribution. Possible short range ordering in the phase equilibrium experiments used in their evaluation might be responsible for the difference to our calorimetrically determined value. This is because short range ordering generates negative excess configurational entropies of mixing, i.e., the short range ordered phase has a somewhat lower S^{cfg} compared to the disordered structure. Ordering phenomena in Ag–Pd alloys were also reported by first principles studies [e.g., 20, 21].

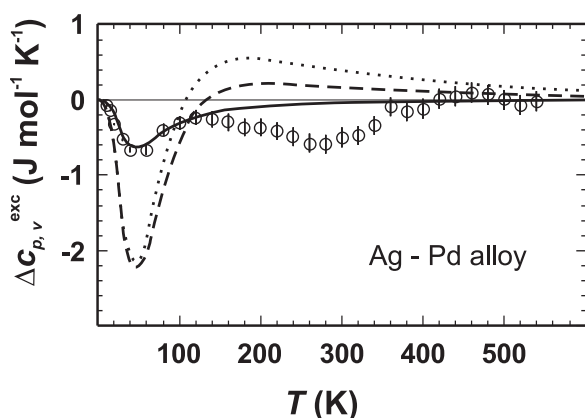


Fig. 2. Measured isobaric excess heat capacity of mixing, $\Delta C_{p,v}^{\text{exc}}$, for $\text{Ag}_{69.7}\text{Pd}_{30.3}$ (open circles with error bars which represent one standard deviation). Lines: Isochoric excess heat capacities of mixing, ΔC_v^{exc} , from DFT calculations (LDA, ultrasoft). Dotted line: DFT results for ordered $\text{Ag}_{75}\text{Pd}_{25}$ (cell 2 in Fig. 3); dashed line: DFT results for disordered $\text{Ag}_{75}\text{Pd}_{25}$ (cell 3 in Fig. 3); solid line: DFT results for ordered $\text{Ag}_{75}\text{Pd}_{25}$ (cell 1 in Fig. 3) including anharmonic contributions (atomic displacement of 0.04 Å).

Table 1

DFT parameter settings used in the final phonon calculations (in cases, where the LDA functional and an ultrasoft pseudopotential were used).

Cut off for plane wave basis set	330 eV
Grid for fast Fourier transform	$24 \times 24 \times 24$
Convergence threshold for self-consistent field	5×10^{-7} eV/atom
Spacing for k -point sampling (electrons)	0.04 \AA^{-1}
Spacing for q -point sampling (phonons)	0.04 \AA^{-1}
Extension of the super cell volume in finite displacement calculations	12 times of the original super cell

3.2. DFT results on the Ag–Pd alloy

Fig. 3 shows the Ag–Pd cells (with $\text{Ag}_{75}\text{Pd}_{25}$ composition) which were investigated by the DFT calculations. Cell 1 and cell 2 differ in their sizes, but have the same configuration, i.e., an ordered Ag–Pd distribution having no Pd–Pd bonds, whereas cell 3 is one of the investigated quasi random structures (disordered Ag–Pd distribution) generated by a Mathematica[®] routine. Using cell 1, the convergence criteria have been worked out yielding DFT parameter settings, of which the most important ones are listed in Table 1. The excess heat capacities converged fast and enabled, for example, a relatively coarse meshed k -point sampling grid to be used. This can be judged from Table 2. The absolute heat capacities and the lattice parameters did not converge so fast. Possible systematic

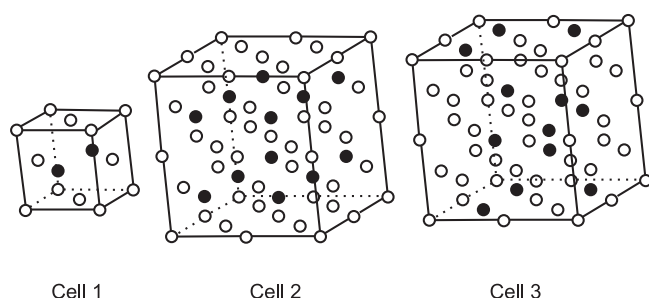


Fig. 3. Configurations of the $\text{Ag}_{75}\text{Pd}_{25}$ alloy used in DFT calculations. Open circles: Ag; closed circles: Pd. Cell 1 and cell 2 have an ordered Ag–Pd distribution, cell 3 has a disordered one.

errors inherent in these values, however, were cancelled out when considering the excess heat capacities of mixing.

The results from DFT calculations are shown in Fig. 2. The excess heat capacities of cell 2 and cell 3 have larger negative peaks at ~ 50 K when compared to the experimental results. Cell 2 and cell 3, however, yielded similar excess heat capacities demonstrating only little dependence on the Ag–Pd distribution. We investigated further cells with disordered configurations, which yielded almost identical results compared to that of cell 3. A small dependence of the heat capacity on cation ordering was also reported for $\text{NaAlSi}_3\text{O}_8$ and KAlSi_3O_8 [22]. A detailed first principles study [23] investigated the effect of chemical order on the vibrational entropy in Ni_3Al and Pd_3V . No such effect was found in Ni_3Al , when the system was relaxed. However, disordering of the ordered Pd_3V phase decreased the vibrational entropy by 1–2% because in ordered Pd_3V , the symmetry constraints prevented the relaxation.

Using cell 1, further phonon calculations were performed. Best agreement with the calorimetric results could be achieved, if the amplitudes for the atomic displacement were increased from the default value of 0.0053 Å to higher values. This allows consideration of anharmonic vibrations that are generated by the asymmetric potential well. An atomic displacement of 0.04 Å improved the agreement with the experimental data significantly (Fig. 2, solid curve). The thermal displacement of ~ 0.04 Å is comparable to experimentally determined values [24]. At a temperature of 75 K, averaged thermal displacements of 0.049 and 0.038 Å for Ag and Pd, respectively, are reported [24] demonstrating consistency with the DFT calculations.

The negative peak in the observed excess heat capacity at 270 K, however, could not be verified by our DFT calculations and the reason for this discrepancy remains unclear. It must be noted that the measured excess heat capacity of mixing is isobaric, whereas in the DFT calculations it is isochoric, which, however, is unlikely to explain the difference at 270 K because unexpected dependences of the thermal expansion coefficient and/or bulk modulus on the temperature and composition would have to be invoked. It is more likely that the discrepancy at 270 K is due to anharmonic vibrations that are related to phonon–phonon interactions. This anharmonic contribution was not considered in the calculations.

So far, the DFT calculations discussed here used an ultrasoft pseudopotential for calculating the wavefunctions of the ion core and LDA as functional. Using the GGA-PBE functional [15], the absolute heat capacities and the lattice parameters differed significantly from the LDA results (Table 3). If, however, the excess heat capacities of mixing were considered, the differences were small, when using an atomic displacement of ~ 0.04 Å. This was also true, if a norm-conserving pseudopotential in combination with LDA was applied. Considering the absolute heat capacity values and the lattice parameters, this combination achieved the best agreement with the observations (Table 3).

3.3. Relationship for estimating the excess vibrational entropy

The relationship, which correlates $\Delta_{\text{max}} S^{\text{exc}}$ linearly with ΔV_i and ΔK_i [10] was applied to the calorimetrically measured excess entropy data on the Pt–Rh and Ag–Pd alloys and to the excess entropy of two alloys (Au–Pt, Ag–Au) reported in Kubashewski and Alcock [1]. We used only these two alloys from Kubashewski and Alcock [1] for our data compilation because no configurational and magnetic contributions to the entropy are to be expected here. Together with the already investigated silicate solid solutions [10], a data set comprising 10 binaries was prepared (Table 4). The ΔV_i and ΔK_i data were calculated from the literature values (see Table 4 for references) and in cases where more than one atom or one molecule was involved in the substitution (i.e.,

Table 2
LDA-DFT convergence criteria for the cell containing 4 atoms (correspondent to cell 1 of Fig. 3). The lattice-parameter (a_0) is given in Å. The heat capacities (C_p , C_v) and the maximum values of the excess heat capacity of mixing ($\Delta_{\max}C_{p,v}^{\text{exc}}$) are given in J mol^{−1} K^{−1}. Those DFT heat capacity results are listed, which used an atomic displacement of 0.04 Å.

	Measured	Spacing for k -point sampling (Å ^{−1})			Cut off for plane wave basis set (eV)		
		0.06	0.04	0.03	300	330	360
$a_0\text{Ag}$	4.086 [41]	4.02	4.01	4.00	4.03	4.01	4.01
$a_0\text{Pd}$	3.890 [41]	3.84	3.84	3.84	3.85	3.84	3.84
$C_{p,v}\text{Ag}$ (100 K)	20.18 [17]	19.9	19.2	19.0	19.6	19.2	19.1
$C_{p,v}\text{Pd}$ (100 K)	17.82 [18]	16.3	15.7	16.1	16.0	15.7	15.7
$\Delta_{\max}C_{p,v}^{\text{exc}}$ (50 K)	−0.65 [this study]	−2.0	−0.6	−0.6	−0.8	−0.6	−0.6

Table 3
DFT results for the cell containing 4 atoms (correspondent to cell 1 of Fig. 3) compared to measured ones. The results for different pseudopotentials (ultrasoft, norm-conserving) and functionals (LDA, GGA-PBE) are listed. The lattice-parameters (a_0) are given in Å. The calculated lattice parameters should principally be smaller than measured ones, because they represent those of lower temperatures (calculated: 0 K; measured: 298 K). However, the difference should be very small (~ 0.01 Å) [26]. The heat capacities (C_p , C_v) and the maximum values of the excess heat capacity of mixing ($\Delta_{\max}C_{p,v}^{\text{exc}}$) are given in J mol^{−1} K^{−1}. C_v should principally be smaller than C_p . However, the difference should again be very small at 50 and 100 K [25]. Those DFT heat capacity results are listed, which used an atomic displacement of ~ 0.04 Å.

	Measured	LDA ultrasoft	LDA norm-conserving	GGA-PBE ultrasoft	Ab initio values from the literature
$a_0\text{Ag}$	4.086 [41]	4.01	4.08	4.15	4.05 [25]
$a_0\text{Pd}$	3.890 [41]	3.84	3.84	3.93	3.91 [26]
$C_{p,v}\text{Ag}$ (50 K)	11.66 [17]	10.4	12.2	12.9	10.0 [25]
$C_{p,v}\text{Ag}$ (100 K)	20.18 [17]	19.2	20.3	20.7	20.0 [25]
$C_{p,v}\text{Pd}$ (50 K)	8.139 [18]	6.0	7.5	7.6	6.9 [26]
$C_{p,v}\text{Pd}$ (100 K)	17.82 [18]	15.7	17.0	17.2	17.5 [26]
$\Delta_{\max}C_{p,v}^{\text{exc}}$ (50 K)	−0.65 [this study]	−0.6	−0.7	−0.8	

$\text{Mg}_3\text{Al}_2\text{Si}_3\text{O}_{12}\text{--Ca}_3\text{Al}_2\text{Si}_3\text{O}_{12}$ and $\text{Mg}_2\text{SiO}_4\text{--Fe}_2\text{SiO}_4$), their ΔV_i and $\Delta_{\max}S^{\text{exc}}$ values were normalised. The observed ΔV_i , ΔK_i , and $\Delta_{\max}S^{\text{exc}}$ data were then used to fit the parameters m and f of the following linear relationship:

$$\Delta_{\max}S^{\text{exc}} = (\Delta V_i + m\Delta K_i)f \tag{2}$$

yielding $m = 0.0109$ and $f = 2.505$. In Fig. 4, ΔV_i is plotted against ΔK_i together with lines of constant maximum excess vibrational entropies. These are positive, if the end-member with the larger volume is elastically stiffer (positive ΔK_i values). Negative vibrational excess entropies are obtained, when the end-member with the larger volume has a much lower bulk modulus compared to the other end-member (large negative ΔK_i values). Ideal vibrational behaviour is proposed, if either the end-members have the same volumes and bulk moduli or an existing volume mismatch is compensated by negative ΔK_i values (see the line with zero $\Delta_{\max}S^{\text{exc}}$ in Fig. 4). The fit parameters from this study are somewhat lower com-

pared to $m = 0.0246$ and $f = 2.926$ obtained when fitting only the data from the silicate solid solutions [10]. It may be assumed that the excess vibrational entropy behaviour of the silicate solid solutions is thus described poorer by the new relationship incorporating the alloys. This, however, is not the case generally, which can be seen in Fig. 5, where the calculated excess vibrational entropy values are plotted against the observed ones. Only the excess vibrational entropy of the plagioclase ($\text{NaAlSi}_3\text{O}_8\text{--CaAl}_2\text{Si}_2\text{O}_8$) solid solution is not well described now (marked by brackets in Fig. 5), whereas in all other cases the predicted and observed excess entropies agree well. The reason for the disagreement with the plagioclases is not known. However, the relationship (Eq. (2)) may be too simple to properly describe the behaviour in complex coupled substitutions. Another problem inherent with Eq. (2) is that solid solutions with a non-significant difference in their end-member volumes are difficult to treat. It is unclear in these cases whether the difference in the bulk moduli has a positive or negative sign.

Table 4
Differences in the end-member volumes and bulk moduli (ΔV_i and ΔK_i), and values for the maximum excess vibrational entropy ($\Delta_{\max}S^{\text{exc}}$). The negative differences in the ΔK_i data are obtained, if the end-member with the larger volume has a lower bulk modulus. The values for ΔV_i and $\Delta_{\max}S^{\text{exc}}$ are normalised to a substitution of one atom or one molecule in the case of a coupled substitution. For $\text{Mg}_3\text{Al}_2\text{Si}_3\text{O}_{12}\text{--Ca}_3\text{Al}_2\text{Si}_3\text{O}_{12}$ and $\text{Mg}_2\text{SiO}_4\text{--Fe}_2\text{SiO}_4$, these values were, therefore, divided by 3 and 2, respectively.

	ΔV_i (J bar ^{−1})	ΔK_i (GPa)	$\Delta_{\max}S^{\text{exc}}$ (J mol ^{−1} K ^{−1})	
			Observed by experiments	Calculated using Eq. (2)
Analbite–sanidine NaAlSi ₃ O ₈ –KAlSi ₃ O ₈	0.86 [27]	8[28,29]	2.6 [2]	2.4
Pyrope–grossular Mg ₃ Al ₂ Si ₃ O ₁₂ –Ca ₃ Al ₂ Si ₃ O ₁₂	0.403 [30,31]	−1[30,31]	1.0 [32]	1.0
Forsterite–fayalite Mg ₂ SiO ₄ –Fe ₂ SiO ₄	0.133 [33]	−6 [34]	0 [35]	0.2
Analbite–anorthite NaAlSi ₃ O ₈ –CaAl ₂ Si ₂ O ₈	0.06 [27,36]	32 [28,37]	2.6 [4]	1.0
Anorthite–sanidine CaAl ₂ Si ₂ O ₈ –KAlSi ₃ O ₈	0.82 [27,36]	−25[28,37]	1.0 [38]	1.3
CaTs–diopside CaAl ₂ SiO ₆ –CaMgSi ₂ O ₆	0.25 [39]	−13 [40]	0[39]	0.3
Au–Pt	0.1124 [41]	−105 [42]	−2.4 [1]	−2.6
Ag–Au	0.0057 [41]	−73 [42]	−1.4 [1]	−2.0
Ag–Pd	0.1412 [41]	−80 [42]	−1.7 [this study]	−1.8
Pt–Rh	0.0811 [41]	8 [42]	0.5 [this study]	0.4

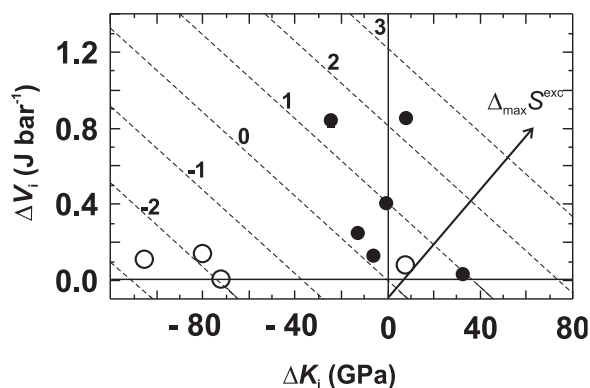


Fig. 4. Difference in normalised end-member volumes (ΔV_i) versus difference in end-member bulk moduli (ΔK_i). Solid symbols: silicate solid solutions; open symbols: alloys. Broken lines represent contours of constant maximum excess vibrational entropy ($\Delta_{\max} S^{\text{exc}}$ ranging from -3 to $3 \text{ J mol}^{-1} \text{ K}^{-1}$). Negative ΔK_i values were obtained if the end-member with the larger volume had a lower bulk modulus.

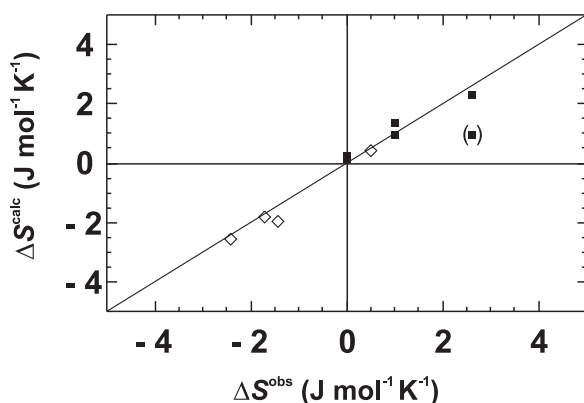


Fig. 5. Calculated excess vibrational entropy (ΔS^{calc}) using Eq. (2) versus measured excess vibrational entropy (ΔS^{obs}). Solid symbols: results from the silicate solid solutions; open symbols: binary alloys. The data point of the plagioclase ($\text{NaAlSi}_3\text{O}_8$ – $\text{CaAl}_2\text{Si}_2\text{O}_8$) solid solution is marked by brackets.

4. Conclusions

A positive excess vibrational entropy was observed for the Pt–Rh alloy, whereas the Ag–Pd alloy is characterised by a negative one, which could also be found by DFT calculations. These calculations showed that the atomic configuration has only a small influence on the heat capacity of the Ag–Pd alloy and that anharmonic effects modify the excess vibrational behaviour.

The relationship presented in Eq. (2) is based on the consideration outlined in the introduction with components AC and BC. It, however, represents a situation, which differs from that in alloys: In AC–BC solid solutions, the polyhedra are mixed, and no new nearest neighbour bonds are generated, which are not already present in the pure substances. The difference of the end-member bulk moduli represents, therefore, the difference in stiffness of the AC_x and BC_x polyhedra at end-member composition. This situation is expected to be similar, if atom C in AC–BC solid solutions is replaced by larger molecules. From this point of view, it seems not surprising, that Eq. (2) is able to describe roughly the magnitude of the excess vibrational entropy of silicate solid solutions (except those with coupled substitutions). However, when mixing elements A and B to form an alloy, new nearest neighbour bonds are generated (A–B bonds), which may have completely different elastic properties than the mean elastic properties of the bonds in the pure phases. Let us consider an alloy, where element A and B are on either side of the transition metals series in the periodic table. In the middle of the

transition metals series, the bulk moduli tend to have a maximum and hence, it is to be expected, that the A–B bonds will be stiffer than the A–A or B–B bonds. This situation was in fact found for the Pd_3V alloy [23].

Eq. (2) is not able to describe such behaviour. Further investigations are therefore planned to work out the limits of this relationship.

Acknowledgments

This work was supported by a grant from the Austrian Science Fund (FWF), project numbers P23056–N21 and P21370–N21, which is gratefully acknowledged. We thank P. Zinterhof, E. Forsthofer and colleagues for their professional work in installing and servicing the Materials Studio software at the Department of Computer Sciences, Salzburg University. We thank also M. Grodzicki, Salzburg, for his valuable contributions.

References

- [1] O. Kubaschewski, C.B. Alcock, Metallurgical Thermochemistry, Pergamon Press, Oxford, 1979.
- [2] H.T. Haselton Jr., G.L. Hovis, B.S. Hemingway, R.A. Robie, Am. Miner. 86 (1983) 398–413.
- [3] H.T. Haselton Jr., E.F. Westrum Jr., Geochim. Cosmochim. Acta 44 (1980) 701–709.
- [4] A. Benisek, E. Dachs, H. Kroll, Am. Miner. 94 (2009) 1153–1161.
- [5] V.T. Witusiewicz, F. Sommer, J. Alloys Compounds 312 (2000) 228–237.
- [6] V.S. Urusov, in: C.A. Geiger (Ed.), Solid Solutions in Silicate and Oxide Systems, EMU Notes in Mineralogy 3, Eötvös University Press, Budapest, 2001, pp. 121–153.
- [7] V.S. Urusov, T.G. Petrova, N.N. Eremin, Crystallogr. Rep. 53 (2008) 1030–1038.
- [8] A. van de Walle, G. Ceder, Rev. Mod. Phys. 74 (2002) 11–45.
- [9] B.P. Burton, A. van de Walle, Chem. Geol. 225 (2006) 222–229.
- [10] A. Benisek, E. Dachs, Phys. Chem. Miner. 38 (2011) 185–191.
- [11] E. Dachs, C. Bertoldi, Eur. J. Miner. 17 (2005) 251–259.
- [12] E. Dachs, A. Benisek, Cryogenics 51 (2011) 460–464.
- [13] S.J. Clark, M.D. Segall, C.J. Pickard, P.J. Hasnip, M.I.J. Probert, K. Refson, M.C. Payne, Z. Kristallogr. 220 (2005) 567–570.
- [14] D.M. Ceperley, B.J. Alder, Phys. Rev. Lett. 45 (1980) 566–569.
- [15] J.P. Perdew, K. Burke, M. Ernzerhof, Phys. Rev. Lett. 77 (1996) 3865–3868.
- [16] S. Wei, M.Y. Chou, Phys. Rev. Lett. 69 (1992) 2799–2802.
- [17] G.T. Furukawa, W.G. Saba, M.L. Reilly, Natl. Stand. Ref. Data Ser. Natl. Bur. Stand. 18 (1968).
- [18] G.T. Furukawa, M.L. Reilly, J.S. Gallagher, J. Phys. Chem. Ref. Data 3 (1974) 163–209.
- [19] I. Barin, O. Knacke, Thermochemical Properties of Inorganic Substances, Springer-Verlag, Berlin, 1973.
- [20] A. Gonis, W.H. Butler, G.M. Stocks, Phys. Rev. Lett. 50 (1983) 1482–1485.
- [21] S. Müller, A. Zunger, Phys. Rev. Lett. 87 (2001) 165502.
- [22] R.E. Openshaw, B.S. Hemingway, R.A. Robie, D.R. Waldbaum, K.M. Krupka, J. Res. U.S. Geol. Surv. 4 (1976) 195–204.
- [23] D. Morgan, A. van de Walle, G. Ceder, J.D. Althoff, D. de Fontaine, Model. Simul. Mater. Sci. Eng. 8 (2000) 295–309.
- [24] L.M. Peng, G. Ren, S.L. Dudarev, M.J. Whelan, Acta Cryst. A 52 (1996) 456–470.
- [25] J. Xie, S. de Gironcoli, S. Baroni, Phys. Rev. B 59 (1999) 965–969.
- [26] Z.L. Liu, J.H. Yang, L.C. Cai, F.Q. Jing, D. Alfe, Phys. Rev. B 83 (2011), pp. 144113–1–144113–9.
- [27] H. Kroll, P.H. Ribbe, in: P.H. Ribbe (Ed.), Feldspar Mineralogy, Reviews in Mineralogy, Mineralogical Society of America, 1983, pp. 57–98.
- [28] N. Curetti, L.M. Sochalski-Kolbus, R.J. Angel, P. Benna, F. Nestola, E. Bruno, Am. Miner. 96 (2011) 383–392.
- [29] R.J. Angel, in: I. Parsons (Ed.), Feldspars and Their Reactions, Kluwer Academic Publishers, Dordrecht, Boston, London, 1994, pp. 271–312.
- [30] C.A. Geiger, Miner. Petrol. 66 (1999) 271–299.
- [31] A. Chopelas, Phys. Chem. Miner. 33 (2006) 363–376.
- [32] E. Dachs, C.A. Geiger, Am. Miner. 91 (2006) 894–906.
- [33] R.G. Schwab, D. Küstner, Neues Jahrbuch fuer Mineralogie–Monatshefte (1977) 205–215.
- [34] D.H. Chung, Geophys. J. R. Astron. Soc. 25 (1971) 511–538.
- [35] E. Dachs, C.A. Geiger, V. von Seckendorff, M. Grodzicki, J. Chem. Thermodyn. 39 (2007) 906–933.
- [36] A. Benisek, H. Kroll, L. Cemič, V. Kohl, U. Breit, B. Heying, Contrib. Miner. Petrol. 145 (2003) 119–129.
- [37] R.J. Angel, Contrib. Miner. Petrol. 147 (2004) 506–512.
- [38] A. Benisek, E. Dachs, H. Kroll, Phys. Chem. Miner. 37 (2010) 209–218.
- [39] K. Etzel, A. Benisek, E. Dachs, L. Cemič, Phys. Chem. Miner. 34 (2007) 733–746.
- [40] M.D. Collins, J.M. Brown, Phys. Chem. Miner. 26 (1998) 7–13.
- [41] R.A. Robie, B.S. Hemingway, J.R. Fisher, Geol. Surv. Bull. 1452 (1978) 1–456.
- [42] K.A. Gschneidner, Solid State Phys. 16 (1964) 275–426.